

# Automated threshold selection and associated inference uncertainty for univariate extremes

Conor Murphy\*, Jonathan A. Tawn

Department of Mathematics and Statistics, Lancaster University

and

Zak Varty

Department of Mathematics, Imperial College London

October 30, 2023

## Abstract

Threshold selection is a fundamental problem in any threshold-based extreme value analysis. While models are asymptotically motivated, selecting an appropriate threshold for finite samples can be difficult through standard methods. Inference can also be highly sensitive to the choice of threshold. Too low a threshold choice leads to bias in the fit of the extreme value model, while too high a choice leads to unnecessary additional uncertainty in the estimation of model parameters. In this paper, we develop a novel methodology for automated threshold selection that directly tackles this bias-variance trade-off. We also develop a method to account for the uncertainty in this threshold choice and propagate this uncertainty through to high quantile inference. Through a simulation study, we demonstrate the effectiveness of our method for threshold selection and subsequent extreme quantile estimation. We apply our method to the well-known, troublesome example of the River Nidd dataset.

*Keywords:* extreme values, generalised Pareto distribution, river flows, return level, threshold selection, uncertainty quantification.

---

\*This paper is based on work completed while Conor Murphy was part of the EPSRC funded STOR-i centre for doctoral training (EP/S022252/1), with part-funding from Shell Research Ltd.

# 1 Introduction

An inherent challenge in risk modelling is the estimation of high quantiles or extrapolation beyond observed levels. This is important when designing policies or protections against future extreme events, e.g., in finance or hydrology (Smith, 2003; Coles et al., 2003). Extreme value methods achieve this extrapolation by using asymptotically exact models to approximate the tail of a distribution above a high within-sample threshold. The first challenge is to select a threshold  $u$ , above which the GPD gives a good approximation to the data. Here, we develop an automatic threshold selection procedure and novel inference methods that account for the uncertainty in this selection. Throughout, we assume all data considered consist of independent, identically-distributed (iid) observations.

To estimate high quantiles of a distribution, known as *return levels*, a single flexible family of distributions can be used. Suppose a univariate continuous random variable  $X$  has distribution function  $F$ , with upper endpoint  $x^F := \sup\{x : F(x) < 1\}$ . When considering values of  $X$  that exceed a high threshold  $u < x^F$ , Pickands (1975) showed that after suitable rescaling, the excesses  $Y = X - u$ , for  $X > u$ , converge in distribution to the generalised Pareto distribution (GPD) as  $u \rightarrow x^F$ . In practice, a suitably high threshold  $u$  must be chosen, so that excesses  $Y$  are well-modelled as  $\text{GPD}(\sigma_u, \xi)$ , which has distribution function

$$H(y; \sigma_u, \xi) = 1 - (1 + \xi y / \sigma_u)_+^{-1/\xi}, \quad (1)$$

with  $y > 0$ ,  $w_+ = \max(w, 0)$ , shape parameter  $\xi \in \mathbb{R}$  and threshold-dependent scale parameter  $\sigma_u > 0$ . For  $\xi = 0$ , distribution (1) is evaluated in the limit as  $\xi \rightarrow 0$ , resulting in

the exponential distribution. For  $\xi < 0$ ,  $X$  has a finite upper end-point at  $u - \sigma_u/\xi$  but is unbounded above for  $\xi \geq 0$ . Davison and Smith (1990) provide an overview of the properties of the GPD and illustrate simple visual threshold selection techniques and diagnostics.

Threshold selection involves a bias-variance trade-off: too low a threshold is likely to violate the asymptotic basis of the GPD model, leading to bias, whilst too high a threshold results in very few threshold excesses with which to fit the model, leading to high parameter uncertainty. Thus, we must choose as low a threshold as possible subject to the GPD providing a reasonable fit to the data. There are a variety of methods aiming to tackle this problem, see Scarrott and MacDonald (2012) for a review and Wadsworth (2016) and Northrop et al. (2017) for recent developments. The most commonly used methods suffer from subjectivity. There are a limited number of existing automated threshold selection methods, and we find our approach compares favourably to these.

When estimating high quantiles, the available data are often few and so inference is sensitive to the chosen threshold. Reliance on a single threshold when accounting for estimation uncertainty is misleading for inference. Using a simple bootstrap procedure together with our threshold selection approach, both threshold and parameter uncertainty are incorporated into tail inference. Our approach builds closely upon that of Varty et al. (2021), adjusting the method to select a constant threshold. Given this, we believe the framework will hold more generally, e.g., with covariate dependence in threshold and/or GPD parameters.

In Section 2, we outline the standard, subjective approaches to threshold selection based on visual assessments. Section 3 describes a number of existing automated methods. Section 4 introduces our procedure for the selection of a threshold, while Section 5 describes how to

incorporate threshold and parameter uncertainty into return level inference. In Section 6, the proposed method is compared against existing methods on simulated data. In Section 7, the River Nidd dataset of Davison and Smith (1990) is used as a non-trivial example and illustrates the superiority of our new methodology relative to the existing methods.

## 2 Background

The *threshold stability property* of the GPD is key in many threshold selection approaches: if excesses of a threshold  $u$  follow a GPD then excesses of a higher threshold  $v$  ( $u < v < x^F$ ) will also follow a GPD, with adjusted parameter values, i.e., if  $X - u | (X > u) \sim \text{GPD}(\sigma_u, \xi)$ , then  $X - v | (X > v) \sim \text{GPD}(\sigma_u + \xi(v - u), \xi)$ , see supplementary material S:2.1 for details. By this property, the GPD shape parameter  $\xi$  should be equal for all valid choices of threshold. A modelling threshold can be selected as the lowest value for which this property holds, accounting for the sampling variability in the estimates of  $\xi$ . The conventional method for this assessment is known as a *parameter stability plot* (Coles, 2001). For each of a set of candidate thresholds, a parameter stability plot displays the estimated  $\xi$  value and the associated confidence interval (CI). The threshold is selected as the lowest value for which the estimate of  $\xi$  for that level is consistent with estimates of  $\xi$  at all higher thresholds, i.e., where there is overlap between the associated CIs.

Figure 1 shows two examples of parameter stability plots; the first uses a simulated dataset of 200 random variates, generated from the Case 4 distribution described in Section 6, where excesses of the threshold  $u = 1.0$  follow a  $\text{GPD}(0.6, 0.1)$ ; the second uses 154 measurements from the River Nidd dataset. Selecting an appropriate threshold using the shape parameter

estimates in Figure 1 is challenging and subjective in both cases because the parameter estimates are dependent across threshold choices and highly uncertain due to the small sample sizes that characterise extreme value analyses. The parameter stability plot for the simulated data shows that values as far from the truth (of  $\xi = 0.1$ ) as  $\xi \approx -0.34$  fall within all CIs, which incorrectly suggests that the entire dataset might be used, i.e., setting  $u = 0$ .

Focusing on the River Nidd dataset one might choose a threshold around the 80%-quantile, implying  $\hat{\xi} \approx -0.1$ . A major drawback to selecting such a high threshold is the high level of uncertainty in the parameter estimates, shown by the wide bootstrap CIs. The parameter stability plot for the Nidd dataset is particularly difficult to interpret because of the large variation in point estimates for  $\xi$  over different threshold choices. Lower candidate threshold values imply a very heavy-tailed distribution ( $\hat{\xi} \approx 0.5$ ), much heavier than is common for almost all published analyses of environmental datasets. Conversely, high thresholds imply a very short tail, with estimates dropping as low as  $\hat{\xi} \approx -1$ . As a result of this unusual behaviour, it has become a major example for non-trivial threshold selection and is analysed in many papers (Tancredi et al., 2006; Wadsworth and Tawn, 2012; Northrop and Coleman, 2014). We apply our new method to this dataset in Section 7. Further examples of parameter stability plots are given in supplementary material S:2.2.

A range of model-based methods have been developed to improve on parameter stability plots for threshold selection. Behrens et al. (2004) treated the threshold as a parameter to be estimated and employed a gamma distribution to model observations below the threshold, which is spliced with the GPD model above the threshold. Tancredi et al. (2006) developed a combined model for both extreme and non-extreme data, using a piecewise-constant den-

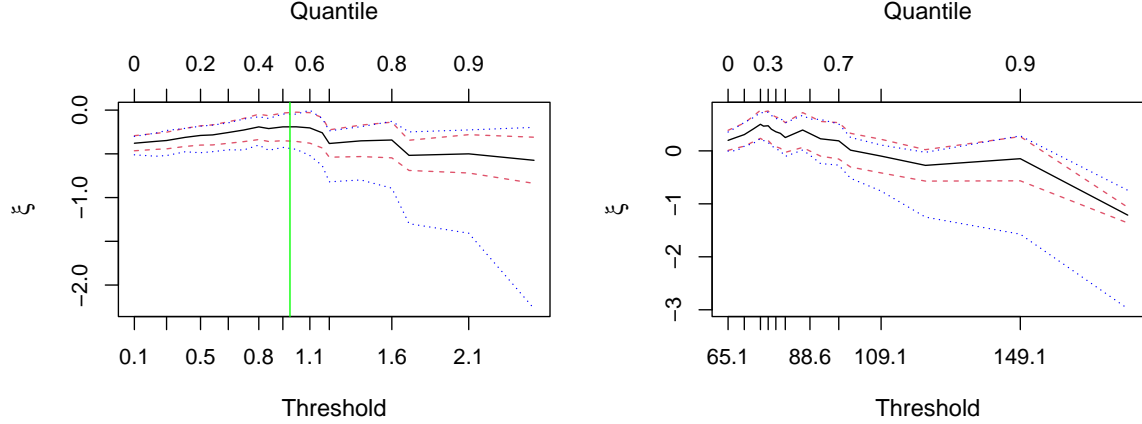


Figure 1: Examples of parameter stability plots with pointwise CIs using the delta-method [dashed] and bootstrapping [dotted] for [left] a simulated dataset with true threshold  $u = 1.0$  and [right] the River Nidd dataset.

sity up to an unknown transition point that is to be estimated along with a GPD density above this point. Wadsworth and Tawn (2012) developed a penultimate non-homogeneous Poisson process (NHPP) model, under which the shape parameter is treated as a piecewise constant function of threshold; a likelihood-based test is used to assess if a single constant shape parameter is appropriate, but this is highly computationally intensive. Northrop and Coleman (2014) built upon this idea, constructing a hypothesis test of a constant shape parameter against a piecewise-constant parameter across an arbitrary number of thresholds. An illustration of this method applied to a simulated dataset from Section 6 is given in supplementary material S:2.3. While this method formalises the approach of parameter stability plots, the resulting plot of  $p$ -values suffers from similar subjectivity of interpretation.

### 3 Current automated methods

Automated methods seek to remove the problem of subjectivity by selecting a threshold based on some metric. Danielsson et al. (2001) select a threshold by minimising the mean squared

error (MSE) of the Hill estimator for  $\xi$  (Hill, 1975) through a double-bootstrap procedure. The first bootstrap stage computes the optimal size  $n_1$  for their second bootstrap stage, where  $n_1 < n$  and  $n$  is the data sample size. To reduce computations, the *tea* package (Ossberger, 2020) fixes  $n_1 = 0.9n$ . Further to the computational intensity, the reliance on asymptotic theory leads to inadequate finite sample performance.

Danielsson et al. (2019) attempts to address the shortcomings of the previous method by using an adaptation of the Kolmogorov-Smirnov statistic to quantify goodness of fit in the tail of the distribution but using quantiles rather than probabilities. This selects the threshold that minimises the *maximum* distance between the empirical and modelled quantiles. This approach has three main shortcomings. Firstly, imposing  $\xi > 0$  precludes its use in applications where variables have light upper tails. Secondly, the largest deviations in model fit are often observed at the very highest quantiles of a distribution, which falsely pushes the threshold too high. Finally, and most critically, the method fails to reward the reduced uncertainty that accompanies a larger sample, leading to unnecessarily high threshold choices.

The automated threshold selection method of Wadsworth (2016) is based on the vector  $\hat{\xi}^*$  of (standardised) increments in the estimates of  $\xi$  between successive ordered candidate thresholds. Above an appropriate threshold for a GPD, the limit distribution for the elements of  $\hat{\xi}^*$  is iid standard normal. Below the appropriate threshold, the distribution of the corresponding elements of  $\hat{\xi}^*$  will be better approximated by a non-standard normal distribution. A changepoint model describing this behaviour is used for  $\hat{\xi}^*$ . By utilising asymptotic theory on the joint distribution of maximum likelihood estimators (MLEs) from overlapping samples of data, a likelihood ratio test is used to assess at which candidate threshold this

changepoint model is most appropriate. An overview is given in supplementary material S:3.1.

The method of Wadsworth (2016) relies on the large sample asymptotic theory of MLEs which restricts the set of candidate threshold choices in practice (due to failure to converge), with this particularly evident for small samples. This leads to considerable sensitivity to the chosen set of candidate thresholds. We also identify substantial problems when  $\xi < 0$ , which is a major restriction. These features are demonstrated through simulation studies and the analysis of the small River Nidd dataset in Sections 6 and 7 respectively.

Northrop et al. (2017) compare the Bayesian predictive density of GPD fits above a fixed validation threshold  $v$ , based on a set of candidate thresholds  $\{u_i\}_{i=1}^k$  where  $v \geq \max(u_1, \dots, u_k)$ . Inferences are averaged over the posterior distribution of parameters in order to incorporate parameter uncertainty for each candidate threshold. Northrop et al. (2017) fit, what they term, a binomial-GPD (BGPD) for each  $u_i$ . The BGPD takes into account the rate of exceedance of the threshold with an extra parameter  $\lambda_u = \mathbb{P}(X > u)$ . They quantify the predictive ability of this model conditionally on being above  $v$ , for each candidate threshold via leave-one-out cross-validation, and choose the candidate threshold which maximises this measure. An overview is given in supplementary material S:3.2.

The Northrop et al. (2017) method requires subjective choices of the validation threshold, the prior density, and the below-threshold model. As defined, the BGPD model is not a valid “density” as it integrates to  $\infty$  and is discontinuous at any candidate threshold. Its results exhibit substantial sensitivity to these choices, e.g., in Section 7 we illustrate this for the choice of  $v$ . Even ignoring the sensitivity due to the subjective choices, we find this

method produces quite variable threshold estimates, see Section 6.

Varty et al. (2021) develop a procedure to select a time-varying threshold  $u(t)$  for earthquake magnitudes. They address a missing data problem by assuming excesses of a constant threshold,  $u_0 < u(t)$  for all  $t$ , are independent  $\text{GPD}(\sigma_{u_0}, \xi)$  random variables. Values exceeding  $u(t)$  are assumed never to be missed whereas, if  $u(t) > u_0$ , values in the interval  $(u_0, u(t))$  are potentially missed such that the distribution of observed excesses of  $u_0$  at time  $t$  is not GPD. A reduction in  $u(t)$  over time  $t$  would correspond to an improved detection of smaller earthquakes. A number of metrics are investigated to quantify the fit of this GPD model, accounting for parameter uncertainty, thus permitting automated selection of  $u(t)$  over  $t$  within a specified parametric family of model choices for  $u(t)$ .

When  $u(t)$  is not constant, its excesses do not share a marginal GPD. To quantify the model fit, Varty et al. (2021) transform the data onto shared margins using an estimated  $u(t)$ , the estimated GPD parameters for excesses of  $u(t)$ , and the probability integral transform. The method also accounts for data rounding. They use the mean absolute deviation from the diagonal of a QQ-plot on Exponential(1) margins to measure fit, with the modelling threshold selected by minimising this average deviation over  $k$  bootstrap replications. The chosen threshold then rewards low bias and little sampling variability in the fitted model.

## 4 Novel metric-based constant threshold selection

We adapt the approach of Varty et al. (2021) to select a constant threshold for continuous, non-missing, iid data. We use a similar QQ-plot-based metric to select a constant value  $u$

above which a GPD model is consistent with the data, but make this comparison on the original scale, i.e., without the transformation to Exponential(1) margins. For clarity, our threshold selection method on the original margins will be referred to as the *expected quantile discrepancy* (EQD) while the method of Varty et al. (2021) will be termed the *Varty method*.

The following makes the difference between the EQD and Varty methods precise. Let  $\mathbf{x}_u = (x_1, \dots, x_{n_u})$  be the sample of excesses of candidate threshold  $u$ . To incorporate sampling variability into the threshold choice, the expected (average) deviation is calculated across bootstrapped samples of  $\mathbf{x}_u$ , denoted  $\mathbf{x}_u^b$  for the  $b^{\text{th}}$  bootstrap sample,  $b = 1, \dots, k$ , for an appropriate choice of  $k$ . Let  $T(x; \sigma, \xi) = F_{\text{Exp}}^{-1}\{H(x; \sigma, \xi)\}$  where  $F_{\text{Exp}}^{-1}$  is the inverse distribution function of an Exponential(1) variable and define  $T(\mathbf{x}_u; \hat{\sigma}_u, \hat{\xi}_u) = \{T(x_1; \hat{\sigma}_u, \hat{\xi}_u), \dots, T(x_{n_u}; \hat{\sigma}_u, \hat{\xi}_u)\}$ . The sample quantile function  $Q(p, \mathbf{x}_u) : [0, 1] \rightarrow \mathbb{R}^+$  is defined as the linear interpolations of the points  $\left\{ \left( \frac{j-1}{n_u}, x_u^{(j)} \right) : j = 1, \dots, n_u \right\}$ , where  $x_u^{(j)}$  is the  $j^{\text{th}}$  order statistic of  $\mathbf{x}_u$  (increasing with  $j$ ). For the two methods, the mean absolute deviation for  $\mathbf{x}_u^b$  is calculated for the probabilities  $\{p_j = j/(m+1) : j = 1, \dots, m\}$  by

$$d_b(u) = \begin{cases} \frac{1}{m} \sum_{j=1}^m \left| \frac{\hat{\sigma}_u^b}{\hat{\xi}_u^b} [(1-p_j)^{-\hat{\xi}_u^b} - 1] - Q(p_j, \mathbf{x}_u^b) \right| & \text{EQD} \\ \frac{1}{m} \sum_{j=1}^m \left| -\log(1-p_j) - Q(p_j, \hat{T}(\mathbf{x}_u^b; \hat{\sigma}_u^b, \hat{\xi}_u^b)) \right| & \text{Varty,} \end{cases} \quad (2)$$

where  $(\hat{\sigma}_u^b, \hat{\xi}_u^b)$  are the estimated GPD parameters fitted to the bootstrapped sample  $\mathbf{x}_u^b$ . The overall measure of fit is  $\hat{d}_E(u) = \frac{1}{k} \sum_{b=1}^k d_b(u)$ . The selected threshold minimises  $\hat{d}_E(u)$  over the set of candidate thresholds. Unless stated otherwise,  $m = 500$  and  $k = 100$  throughout.

In supplementary material S:4.1, a small simulation study found that for iid data, the EQD

outperforms the Varty method in threshold selection and subsequent quantile inference. The Varty method produced lower threshold choices, resulting in additional bias without sufficient variance reduction to offset this. Thus, in Section 6, we focus on comparison of the EQD against the Wadsworth (2016) and Northrop et al. (2017) methods.

## 5 Accounting for parameter and threshold uncertainty

Even in cases where a true threshold is known, relying on point estimates for the parameters of the fitted model could result in misleading inference (Coles and Pericchi, 2003). CIs can be obtained using the standard error or profile likelihood. However, both methods rely on asymptotic arguments and since threshold exceedances tend to be sparse, bootstrap methods are preferable. Algorithm 1 details a standard parametric bootstrapping procedure to account for parameter uncertainty when the threshold is known. We first fit a GPD to the  $n_u$  excesses of the known threshold  $u$  from a total sample of size  $n$  ( $n \geq n_u$ ). Using the fitted parameters, we simulate  $m_1$  GPD bootstrap samples of  $n_u$  excesses of  $u$ , and re-estimate the parameters for each sample. A summary statistic of interest  $s(\sigma_u, \xi, \lambda_u)$ , e.g., a high quantile, may be computed for each parametric bootstrap to obtain the relevant bootstrap sampling distribution, where  $(\sigma_u, \xi)$  are the GPD parameters as defined in distribution (1) and  $\lambda_u$  is the rate of exceedance of threshold  $u$ <sup>1</sup>. This enables the construction of CIs which represent sampling variability of the GPD parameter estimates.

GPD inferences are sensitive to the choice of threshold (Davison and Smith, 1990) but un-

---

<sup>1</sup>In Algorithm 1, we focus on the uncertainty of the estimates of  $(\sigma_u, \xi)$ . Uncertainty in estimates of  $\lambda_u$  could also be incorporated by simulating a number of excesses drawn from a  $\text{Bin}(n, \lambda_u)$  distribution for each bootstrap. This uncertainty is included in Algorithm 2.

---

**Algorithm 1** Parameter uncertainty for known threshold

---

Fit a GPD above  $u$  and obtain estimates  $(\hat{\sigma}_u, \hat{\xi})$  and  $\hat{\lambda}_u = \mathbb{P}(X > u) = n_u/n$ .

**Require:**  $(\hat{\sigma}_u, \hat{\xi}, \hat{\lambda}_u, n_u, m_1)$

**for**  $b = 1, \dots, m_1$  **do**

- Simulate GPD( $\hat{\sigma}_u, \hat{\xi}$ ) sample  $\mathbf{y}_u^b$  consisting of  $n_u$  excesses of  $u$ .
- Obtain parameter estimates  $(\hat{\sigma}_b, \hat{\xi}_b)$  for  $\mathbf{y}_u^b$  and summary of interest  $s(\hat{\sigma}_b, \hat{\xi}_b, \hat{\lambda}_u)$ .

**end for**

**return** A set of  $m_1$  bootstrapped estimates for the summary statistic of interest.

---

certainty about this choice is not represented in Algorithm 1. This is particularly important when  $s(\sigma_u, \xi, \lambda_u)$  informs the design of hazard protection mechanisms, where omitting the uncertainty in the threshold choice could lead to overconfidence in the resulting estimates and have potentially dangerous consequences. Algorithm 2 provides a novel method to propagate both threshold and parameter uncertainty through to return level estimation, using a double-bootstrap procedure. To focus on the threshold uncertainty and to forgo the need for a parametric model below the threshold, we employ a non-parametric bootstrap procedure on the original dataset. We resample with replacement  $n$  values from the observed data  $m_2$  times, estimate a threshold for each such bootstrap sample using the automated selection method of Section 4, and fit a GPD to the excesses of this threshold. For each one of the  $m_2$  samples, we employ Algorithm 1 to account for the subsequent uncertainty in the GPD parameters. Calculating a summary statistic for each of the  $m_1 \times m_2$  samples leads to a distribution of bootstrapped estimates that accounts for both threshold and parameter uncertainty. Unless stated otherwise,  $m_1 = m_2 = 200$  throughout. In Section 6 we illustrate how using Algorithm 2 improves the coverage probability of CIs, and in Section 7 how it widens CIs for return levels of the River Nidd by accounting for threshold uncertainty.

---

**Algorithm 2** Parameter uncertainty for unknown threshold

---

**Require:**  $(\mathbf{x}, n, m_2, m_1)$

**for**  $b = 1, \dots, m_2$  **do**

    Obtain sample  $\mathbf{x}_b$  of size  $n$  by sampling  $n$  times with replacement from  $\mathbf{x}$ .

    Estimate threshold  $\hat{u}_b$  for  $\mathbf{x}_b$  and record number of excesses as  $n_{\hat{u}_b}$ .

    Employ Algorithm 1 with inputs:  $(\mathbf{x}_b, \hat{u}_b, n, n_{\hat{u}_b}, m_1)$ .

**end for**

**return** A set of  $m_1 \times m_2$  bootstrapped estimates for the summary statistic of interest.

---

## 6 Simulation Study

### 6.1 Overview

We illustrate the performance of the EQD method against the Wadsworth (2016) and Northrop et al. (2017) approaches, which we term the *Wadsworth* and *Northrop* methods respectively. The approaches of Danielsson et al. (2001) and Danielsson et al. (2019) performed considerably worse than all others in threshold selection and quantile estimation; results for these methods are given in supplementary material S:4.4.

To conduct this simulation study, we utilised the following R code. For the Wadsworth method, code is available in the supplementary materials of Wadsworth (2016). For the Northrop method, we used the R package *threshr* (Northrop and Attalides, 2020). For the results given in supplementary material S:4.4, we utilised the *tea* package (Ossberger, 2020) for the Danielsson et al. (2001) method. Note that the package was not built by the authors of the paper. We constructed our own function for the Danielsson et al. (2019) method as there did not seem to be code freely available. R code to implement the EQD method and the analyses throughout this paper can be found at [https://github.com/conor-murphy4/](https://github.com/conor-murphy4/threshold_selection_paper)  
`threshold_selection_paper`.

We assess the performance of each method in two scenarios: one where a true threshold exists and the other where it does not exist but the true quantiles are computable. The comparison is based on the methods' ability to estimate the true threshold (when this exists) and high marginal quantiles. We use the root-mean-square error (RMSE) as a measure of performance. The true quantiles are given in supplementary material S:4.2 and all bias-variance components of RMSE, discussed in this section, are in supplementary material S:4.4.

For data that are GPD above a true threshold  $u$ , excesses of all candidate thresholds above  $u$  will follow a GPD but selecting these thresholds leads to less precise GPD parameter estimates. In contrast, thresholds which are selected below  $u$  lead to bias in the GPD fit as the distribution below  $u$  is not a GPD. So, we would anticipate some positive bias in threshold selection, with the level of this bias dependent on how different the distribution below the threshold is to the GPD above the threshold. This is particularly relevant for Scenario 1 where there is a true threshold.

## 6.2 Scenario 1: True GPD tail

Within Scenario 1, we consider four cases, combining different properties above and below the threshold, with the true threshold being  $u = 1.0$  in all cases. Table 1 provides a model description for each case as well as the average sample size. Case 1 is the simplest due to the clearly defined true threshold, large sample size and positive shape parameter. Case 2 consists of samples generated from the same distribution but with a smaller sample size. Case 3 has double the sample size of Case 1 and a negative  $\xi$ , close to zero. The Wadsworth method failed to estimate a threshold in samples with  $\xi < -0.05$  irrespective of sample size.

Case 3 therefore considers  $\xi = -0.05$  with 2000 exceedances of  $u$ , as required for that method to work reasonably. Further case studies, using samples where the Wadsworth method failed to estimate any thresholds, are provided in supplementary material S:4.3. Cases 1-3 all have a distinct changepoint in the density at the true threshold. Case 4 provides a more difficult example. The data are derived from a partially observed GPD, denoted  $\text{GPD}_p$ , with data from a GPD above 0 and rejected if points lay below an independent random variate from a Beta distribution on  $(0, 1)$ . Thus, conditional on a  $\text{GPD}_p$  variable being above 1, the excesses of 1 follow a GPD.

The results are based on analysis of 500 replicated samples for each case. For each simulated dataset, we tested the set of candidate thresholds  $\{u_i\}_{i=1}^k$ ,  $k = 20$ , corresponding to sample quantile levels of 0%, 5%,  $\dots$ , 95% in each replicated dataset, with the true threshold corresponding to the 16.67% quantile for Cases 1-3 and the 52.5% quantile for Case 4.

Models	Below threshold	Average sample size	Above threshold	Average sample size
Case 1	$U(0.5, 1.0)$	200	$\text{GPD}(0.5, 0.1)$	1000
Case 2	$U(0.5, 1.0)$	80	$\text{GPD}(0.5, 0.1)$	400
Case 3	$U(0.5, 1.0)$	400	$\text{GPD}(0.5, -0.05)$	2000
Case 4	$\text{GPD}_p(0.5, 0.1)$	525	$\text{GPD}(0.6, 0.1)$	475

Table 1: Model specifications for Cases 1-4. In Cases 1-3, the sample size is exact while in Case 4, the amount of data above and below the threshold varies across samples.

**Threshold recovery:** Table 2 shows the RMSE of the chosen thresholds for each method. The EQD achieves RMSEs between 1.9 and 8.0 times smaller than the Wadsworth method and between 4.8 and 9.9 times smaller than the Northrop method. The EQD has the lowest bias and variance in all cases. As for Case 2, the failure rate of the Wadsworth method is so large, RMSEs were also derived solely based on samples where the method estimated a

threshold. The RMSEs calculated using only these samples showed an increased differential in favour of the EQD method relative to that reported in Table 2. Table 3 shows the RMSEs of threshold choice calculated on 500 replicated samples from Case 1 with a larger sample size of  $n = 20000$ . The results are shown for each method using two different candidate grids of thresholds. In contrast to the previous results, the Wadsworth method slightly outperforms the EQD achieving the smallest RMSEs for these large samples. However, the sample size for this to be achieved significantly exceeds that for data in practice. This illustrates the potential benefits, but also serious limitations, of relying on asymptotic methods to guide threshold selection.

	<i>EQD</i>	<i>Wadsworth</i> <sup>2</sup>	<i>Northrop</i>
Case 1	<b>0.048</b>	0.349	0.536
Case 2	<b>0.060</b>	0.461	0.507
Case 3	<b>0.060</b>	0.221	0.463
Case 4	<b>0.101</b>	0.411	0.497

Table 2: RMSE of the threshold choices for each method-case combination. The smallest values for each case are highlighted in bold.

Grid (% quantile)	<i>EQD</i>	<i>Wadsworth</i>	<i>Northrop</i>
0 (5) 95	0.036	<b>0.021</b>	0.503
0 (0.5) 95	0.027	<b>0.003</b>	0.529

Table 3: RMSE of the threshold choices for Case 1 with  $n=20000$  for two different candidate grids given with notation *start (increment) end*. The smallest values are in bold.

**Quantile recovery:** Table 4 presents the RMSEs for the  $(1 - p_j)$ -quantiles where  $p_j = 1/(10^j n)$  for  $j = 0, 1, 2$  with  $n$  denoting the size of the simulated sample. We use exceedance probabilities of this form to ensure that, for all  $n$ , extrapolation is equally difficult. For  $j = 0$ , extrapolation is not required and so, the choice of threshold should not be too important;

---

<sup>2</sup>Results for Wadsworth are calculated only on the samples where a threshold was estimated. It failed to estimate a threshold for 2.4%, 26.4%, 0%, 4.6% of the simulated samples in Cases 1-4, respectively.

the similar RMSEs across methods reflect this, yet as  $j$  increases, all RMSEs increase and the differences between methods become clear. In each case and across all quantiles, the EQD method is best uniformly, followed by the Wadsworth and then, the Northrop method. This pattern reflects the findings in Table 2, although here, the differential performances depend on  $j$ . The EQD achieves the lowest bias in the majority of cases and quantiles and shows considerably less variance in quantile estimates in all cases, particularly as  $j$  increases. However, there are cases (Case 3 in particular) where the Wadsworth method lies close to the EQD method in terms of RMSE. Table 5 shows the RMSEs of quantile estimation for  $n = 20,000$  in Case 1, where for threshold selection the Wadsworth method has a slight benefit over EQD. Here, for quantile estimation, there are similar findings, the Wadsworth method achieves the lowest RMSEs, followed closely by the EQD and then, the Northrop method which obtains significantly higher RMSEs.

	<i>EQD</i>	<i>Wadsworth</i> <sup>2</sup>	<i>Northrop</i>	<i>EQD</i>	<i>Wadsworth</i> <sup>2</sup>	<i>Northrop</i>
<i>j</i>	Case 1			Case 2		
0	<b>0.563</b>	0.594	0.755	<b>0.599</b>	0.631	0.736
1	<b>1.258</b>	1.391	2.376	<b>1.488</b>	1.644	3.513
2	<b>2.447</b>	2.717	7.097	<b>3.119</b>	3.484	22.916
	Case 3			Case 4		
0	<b>0.190</b>	0.195	0.230	<b>0.686</b>	0.777	0.859
1	<b>0.323</b>	0.344	0.450	<b>1.650</b>	1.996	2.760
2	<b>0.483</b>	0.516	0.744	<b>3.370</b>	4.216	8.787

Table 4: RMSEs in the estimated quantiles in Cases 1-4 based on fitted GPD above chosen threshold. The smallest RMSE for each quantile are highlighted in bold.

Grid	0 (5) 95			0 (0.5) 95		
$j$	$EQD$	<i>Wadsworth</i>	<i>Northrop</i>	$EQD$	<i>Wadsworth</i>	<i>Northrop</i>
0	0.370	<b>0.364</b>	0.546	0.369	<b>0.358</b>	0.573
1	0.694	<b>0.681</b>	1.157	0.692	<b>0.669</b>	1.200
2	1.199	<b>1.174</b>	2.189	1.196	<b>1.151</b>	2.242

Table 5: RMSEs in the estimated quantiles in Case 1 samples with  $n = 20000$  based on fitted GPD above chosen threshold for two candidate grids given with notation *start (increment) end*. The smallest RMSE for each quantile are highlighted in bold.

**True quantile coverage:** To demonstrate the merit of including the uncertainty in threshold selection in our inference, we apply Algorithms 1 and 2 to data from Case 4. Table 6 presents the coverage probabilities of the nominal 80% and 95% CIs of the estimated  $(1-p_j)$ -quantiles over the 500 samples. Incorporating only parameter uncertainty (*Alg 1*) leads to underestimation of interval widths and inadequate coverage of the true quantiles, especially as we extrapolate further. The inclusion of the additional threshold uncertainty (*Alg 2*) leads to more accurate coverage of the true quantiles (particularly for the nominal 95% CIs) across all exceedance probabilities, with the coverage probabilities rising to being slightly above the confidence level in each case.

$j$	80% confidence			95% confidence		
	0	1	2	0	1	2
<i>Alg 1</i>	0.752	0.746	0.750	0.902	0.888	0.886
<i>Alg 2</i>	0.876	0.872	0.870	0.970	0.968	0.964

Table 6: Coverage probabilities for estimated quantiles using Algorithm 1 and 2 for 500 replicated samples from Case 4 with sample size of 1000.

### 6.3 Scenario 2: Gaussian data

In applications, there is no true or known value for the threshold, so here, we explore the case where there is no threshold above which excesses follow a GPD. It is well known that Gaussian

tails have very slow convergence towards an extreme value limit (Gomes, 1994) yet for the standard form of this distribution, the true  $(1-p)^{\text{th}}$  quantiles are simply  $\Phi^{-1}(1-p)$ . Therefore, Gaussian data are likely to be particularly difficult for threshold selection but methods can be easily assessed via resultant high quantile estimation. We simulate 500 samples, separately for  $n$  ( $n = 2000$  and  $20000$ ) iid standard Gaussian random variables and use candidate thresholds at sample quantile levels of  $50\%, 55\%, \dots, 95\%$  and  $50\%, 50.5\%, \dots, 95\%$  for the smaller and larger samples respectively. Lower candidate thresholds are unnecessary as the GPD density is monotonically decreasing in contrast to the Gaussian below its mode.

**Quantile recovery:** Table 7 shows the RMSEs of the estimated  $(1-p_j)$ -quantiles where  $p_j = 1/(10^j n)$ , for  $j = 0, 1, 2$  and  $n = 2000, 20000$ . For  $n = 2000$ , the EQD method achieves the smallest RMSE with the Northrop method in second followed by the Wadsworth method. For  $n = 20000$ , the Northrop methods performs best, closely followed by the EQD and then, the Wadsworth method. The median and 95% CI of the chosen thresholds for each method are given in supplementary material S:4.4. The Northrop method tends to choose slightly higher thresholds than the EQD method in both cases, which leads to a small reduction in bias but for only the smaller  $n$  is the additional variability relative to the EQD a disadvantage. The Wadsworth method incurs significantly more bias due to finding lower thresholds in general.

**True quantile coverage:** We are also interested in assessing the coverage of true quantiles using Algorithms 1-2 for Gaussian data. Table 8 presents the coverage probabilities of the nominal 80% and 95% CIs of the estimated  $(1-p_j)$ -quantiles with  $n = 2000$ . *Alg 1* leads to

---

<sup>3</sup>Results for the Wadsworth method, which failed on 0.4% of the samples here, are calculated only for samples where a threshold estimate was obtained.

$j$	$n = 2000$			$n = 20000$		
	$EQD$	$Wadsworth^3$	$Northrop$	$EQD$	$Wadsworth$	$Northrop$
0	<b>0.214</b>	0.249	0.225	0.187	0.214	<b>0.172</b>
1	<b>0.430</b>	0.538	0.461	0.368	0.422	<b>0.331</b>
2	<b>0.703</b>	0.896	0.765	0.594	0.672	<b>0.533</b>

Table 7: RMSEs of estimated  $(1 - p_j)$ -quantiles for 500 replicated samples from a Gaussian distribution with sample size of 2000 and 20000 (on a 0.5% candidate grid) respectively. The smallest RMSE for each quantile are highlighted in bold.

drastic underestimation of uncertainty shown by the very low coverage probabilities at both nominal confidence levels. The added threshold uncertainty results in significant increases in coverage of the true quantiles across the 500 samples. While these fall short of the nominal confidence level, this is to be expected due to the known slow convergence of Gaussian data and the large increase in coverage demonstrates the importance of including this additional uncertainty in inference.

$j$	80% confidence			95% confidence		
	0	1	2	0	1	2
<i>Alg 1</i>	0.588	0.448	0.364	0.750	0.618	0.510
<i>Alg 2</i>	0.718	0.598	0.492	0.866	0.814	0.756

Table 8: Coverage probabilities for estimated  $(1 - p)$ -quantiles using Algorithm 1 and 2 for 500 replicated samples from a Gaussian distribution with sample size of 2000.

## 7 Application to river flow data

The widely-studied River Nidd dataset consists of all 154 observed peak daily river flow rates that exceeded  $65 \text{ m}^3/\text{s}$  in the period 1934-1969. Each observation can therefore be deemed “extreme”, though not necessarily well-described by a GPD. Davison and Smith (1990) describes the preprocessing applied to the data so that observations can be treated as independent and the difficulties this dataset presents for threshold selection and parameter

uncertainty which we reiterated in discussion of Figure 1.

For the EQD method, we use sample percentiles as candidate thresholds (0%, 1%, ..., 99%) and  $k = 200$  bootstrap samples for each candidate threshold. The EQD provides a robust estimate  $\hat{u} = 67.10$ , lower than previous analyses which allows the use of far more exceedances in the extreme value analysis, reducing the uncertainty in parameter estimates and subsequent quantile estimation. The Wadsworth and Northrop methods fail to estimate a threshold on this grid due to convergence issues. Table 9 shows the selected thresholds of each of the methods on a range of different candidate grids<sup>4</sup>. The Wadsworth method fails to estimate a threshold for a dataset of this size unless the candidate grid is made very coarse. This is problematic in practice as using a coarse grid of candidate thresholds is likely to remove the most appropriate threshold from consideration. The Northrop method exhibits substantial variability in the estimated thresholds as the candidate grid is adjusted and requires the grid to be bounded at the validation threshold of the 90%-quantile (if that level is increased, the method either fails or provides convergence warnings). The EQD, however, shows only small variations in the threshold choice as the candidate grid changes, owing to bootstrap sampling variability, however this can be controlled by increasing  $k$ .

Figure 2 shows a QQ-plot for the GPD model using the EQD threshold estimate of  $\hat{u} = 67.10$ . The tolerance bounds (shaded) show a reasonable agreement between model and data. Figure 2 also shows the  $T$ -year return level estimates calculated for this threshold, with  $T \in \{1, \dots, 1000\}$ . The 95% CIs incorporate parameter uncertainty alone (dark-shaded) and both parameter and threshold uncertainty (light-shaded) using Algorithm 1 and 2 respectively,

---

<sup>4</sup>In marked cases, the Northrop method outputted a chosen threshold with some convergence warnings.

Estimated thresholds for the River Nidd dataset			
Grid (% quantile)	EQD	Wadsworth	Northrop
0 (1) 98	67.10 (3%)	NA	111.63 <sup>4</sup> (82%)
0 (1) 90	67.10 (3%)	NA	65.08 (0%)
0 (1) 80	67.10 (3%)	NA	100.28 (75%)
0 (20) 80	65.08 (0%)	NA	109.08 (80%)
0 (30) 90	65.08 (0%)	149.10 (90%)	65.08 (0%)
0 (25) 75	65.08 (0%)	100.28 (75%)	81.53 (50%)
0, 10, 40, 70	65.08 (0%)	65.08 (0%)	69.74 (10%)

Table 9: River Nidd dataset selected thresholds (and quantile %) for each method for different grids of candidate thresholds. The Grid column gives *start (increment) end* for each grid.

with a substantial increase in uncertainty from the latter for larger  $T$ ; e.g., for the 100- and 1000-year return levels, the CI width increases by a factor of 1.38 and 1.52 respectively. This reiterates how vital it is to incorporate threshold uncertainty into inference.

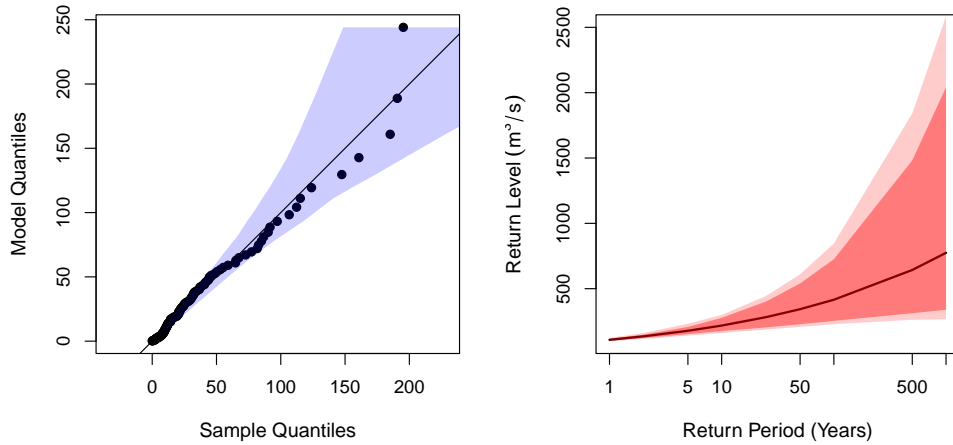


Figure 2: River Nidd analysis: QQ-plot [left] showing model fit with 95% tolerance bounds [shaded] and return level plot [right] based on EQD threshold choice with 95% CIs incorporating parameter uncertainty [dark-shaded] and additional threshold uncertainty [light-shaded].

## 8 Conclusions

We proposed a novel and simple approach (EQD) for automatic threshold selection and a technique to propagate uncertainty in the threshold choice in inference. We compared the EQD method to existing threshold selection methods on the basis of threshold selection and high quantile estimation for iid, continuous data and illustrated its superiority across examples using a range of metrics. We have shown the greater robustness of our method, relative to existing approaches, to changes in the candidate threshold set and demonstrated that incorporating threshold uncertainty with parameter uncertainty improves coverage properties in return level inference. The EQD method avoids many of the shortcomings relating to reliance on asymptotic theory or sensitivity to subjective choices made prior to threshold selection. While this paper has demonstrated the effectiveness of the EQD method in the iid setting, its simple nature leaves it open for easy adjustment for more complex settings.

## References

Behrens, C. N., Lopes, H. F., and Gamerman, D. (2004). Bayesian analysis of extreme events with threshold estimation. *Statistical Modelling*, 4(3):227–244.

Coles, S. G. (2001). *An Introduction to Statistical Modeling of Extreme Values*. Springer, New York.

Coles, S. G. and Pericchi, L. R. (2003). Anticipating catastrophes through extreme value modelling. *Journal of the Royal Statistical Society: Series C (Applied Statistics)*, 52(4):405–416.

Coles, S. G., Pericchi, L. R., and Sisson, S. (2003). A fully probabilistic approach to extreme rainfall modeling. *Journal of Hydrology*, 273(1-4):35–50.

Danielsson, J., de Haan, L., Peng, L., and de Vries, C. G. (2001). Using a bootstrap method to choose the sample fraction in tail index estimation. *Journal of Multivariate Analysis*, 76(2):226–248.

Danielsson, J., Ergun, L., de Haan, L., and de Vries, C. G. (2019). Tail index estimation: quantile-driven threshold selection. Staff Working Papers 19-28, Bank of Canada.

Davison, A. C. and Smith, R. L. (1990). Models for exceedances over high thresholds (with discussion). *Journal of the Royal Statistical Society: Series B*, 52(3):393–425.

Gelfand, A. E. (1996). Model determination using sampling-based methods. *Markov Chain Monte Carlo in Practice*, 4:145–161.

Gomes, M. I. (1994). Penultimate behaviour of the extremes. *Extreme Value Theory and Applications: Proceedings of the Conference on Extreme Value Theory and Applications, Gaithersburg Maryland 1993*, 1:403–418.

Hill, B. M. (1975). A simple general approach to inference about the tail of a distribution. *The Annals of Statistics*, 3(5):1163–1174.

Northrop, P. J. and Attalides, N. (2020). *threshr: Threshold Selection and Uncertainty for Extreme Value Analysis*. R package version 1.0.3.

Northrop, P. J., Attalides, N., and Jonathan, P. (2017). Cross-validatory extreme value

threshold selection and uncertainty with application to ocean storm severity. *Journal of the Royal Statistical Society: Series C (Applied Statistics)*, 66(1):93–120.

Northrop, P. J. and Coleman, C. L. (2014). Improved threshold diagnostic plots for extreme value analyses. *Extremes*, 17(2):289–303.

Ossberger, J. (2020). *tea: Threshold Estimation Approaches*. R package version 1.1.

Pickands, J. (1971). The two-dimensional Poisson process and extremal processes. *Journal of Applied Probability*, 8(4):745–756.

Pickands, J. (1975). Statistical inference using extreme order statistics. *Annals of Statistics*, 3(1):119–131.

Scarrott, C. and MacDonald, A. (2012). A review of extreme value threshold estimation and uncertainty quantification. *REVSTAT–Statistical Journal*, 10(1):33–60.

Smith, R. L. (1987). Approximations in extreme value theory. Technical report, No. 205, Department of Statistics, Univeristy of North Carolina.

Smith, R. L. (2003). Statistics of extremes, with applications in environment, insurance, and finance. In *Extreme Values in Finance, Telecommunications, and the Environment*, edited by Finkenstadt, B. and Rootzén, H., pages 20–97. Chapman and Hall/CRC.

Tancredi, A., Anderson, C. W., and O'Hagan, A. (2006). Accounting for threshold uncertainty in extreme value estimation. *Extremes*, 9(2):87–106.

Varty, Z., Tawn, J. A., Atkinson, P. M., and Bierman, S. (2021). Inference for extreme earthquake magnitudes accounting for a time-varying measurement process. *arXiv:2102.00884*.

Wadsworth, J. L. (2016). Exploiting structure of maximum likelihood estimators for extreme value threshold selection. *Technometrics*, 58(1):116–126.

Wadsworth, J. L. and Tawn, J. A. (2012). Likelihood-based procedures for threshold diagnostics and uncertainty in extreme value modelling. *Journal of the Royal Statistical Society: Series B*, 74(3):543–567.

# Supplementary materials for “Automated threshold selection and associated inference uncertainty for univariate extremes”

Conor Murphy, Jonathan A. Tawn

Department of Mathematics and Statistics, Lancaster University

and

Zak Varty

Department of Mathematics, Imperial College London

## S:1 Introduction

This document provides further information to accompany the main paper. Section S:2 includes derivations of key properties, further description of methods and additional experiments using some of the standard methods for threshold selection, referenced in Section 2 of the main paper. In Section S:3, we provide more detailed descriptions of the Wadsworth (2016) and Northrop et al. (2017) methods analysed in the main paper. Section S:4 presents additional simulation experiments and a detailed breakdown of the results outlined in Section 6 of the main paper.

## S:2 Background for Section 2 material

This section provides further description, examples and derivations of some of the important aspects discussed in Section 2 of the main text.

## S:2.1 Threshold stability property

The threshold stability property provides the basis for the standard threshold selection methods described in Section 2 in the main text. This property is derived as follows. Suppose we have that excesses above a threshold  $u$  follow a GPD such that  $X - u|X > u \sim \text{GPD}(\sigma_u, \xi)$ . We want to find the distribution of excesses of a higher threshold  $v > u$ . Thus, to find the distribution of  $X - v|X > v$  for  $v$  such that  $u < v < x^F$ , where  $x^F$  is the upper endpoint of the distribution of  $X$  and  $x > 0$ , we have:

$$\begin{aligned}
\mathbb{P}(X - v > x|X > v) &= \frac{\mathbb{P}(X > v + x)}{\mathbb{P}(X > v)} = \frac{\mathbb{P}(X > v + x, X > u)}{\mathbb{P}(X > v, X > u)} \\
&= \frac{\mathbb{P}(X > v + x|X > u)}{\mathbb{P}(X > v|X > u)} \\
&= \frac{\left[1 + \frac{\xi(v+x-u)}{\sigma_u}\right]_+^{-1/\xi}}{\left[1 + \frac{\xi(v-u)}{\sigma_u}\right]_+^{-1/\xi}} \quad (\text{as } X - u|X > u \sim \text{GPD}(\sigma_u, \xi)) \\
&= \left[1 + \frac{\xi x}{\sigma_u + \xi(v-u)}\right]_+^{-1/\xi}.
\end{aligned}$$

This is the survivor function of a GPD with scale and shape parameters  $(\sigma_u + \xi(v-u), \xi)$  respectively. Thus,  $X - v|X > v \sim \text{GPD}(\sigma_u + \xi(v-u), \xi)$ .

## S:2.2 Parameter stability plots

Figure S.1 provides three further examples of parameter stability plots to accompany Figure 1 of the main text. The results come from three simulated datasets used in Section 6 of the main paper. These datasets all have true underlying threshold at  $u = 1.0$ , plotted as a vertical red dashed line. The sample sizes of the data analysed in the plots are  $n = 1200, 480, 1000$

from left to right. The three datasets were assessed for stability in the shape parameter estimates  $\hat{\xi}$  for a grid of threshold choices at sample quantile levels of 0%, 5%,  $\dots$ , 95%. The first and third plot seem to show approximate stability above the true threshold. However, the increasing uncertainty as the threshold choice is raised demonstrates the difficulty in objectively assessing this stability. This difficulty is more evident in the second plot of Figure S.1 due to the smaller sample size for these data. The smaller sample size, which is certainly not unusually small for an extreme value analysis, results in highly variable parameter estimates across thresholds and a level of uncertainty which makes the visual assessment of stability difficult. These simulated examples are cases where the underlying true threshold should be fairly clear, and yet, it is not a straightforward task to make appropriate inferences from the parameter stability plots. When using this method to assess the stability of parameter estimates derived from real data, subjective choices of threshold can lead to inefficient or biased inference.

The major criticism of the parameter stability plots is their lack of interpretability, since pointwise confidence intervals are highly dependent across the set of thresholds and, thus, are difficult to account for when assessing stability (see e.g., Wadsworth and Tawn (2012); Northrop and Coleman (2014); Wadsworth (2016)). It is also important to note that the parameter stability plot relies heavily on the choice of the grid of threshold choices that we compare. Estimates of the shape parameter and confidence intervals are only evaluated at each threshold choice in the grid so interpretation of a parameter stability plot and thus, the threshold choice will be sensitive to the grid of candidate thresholds.

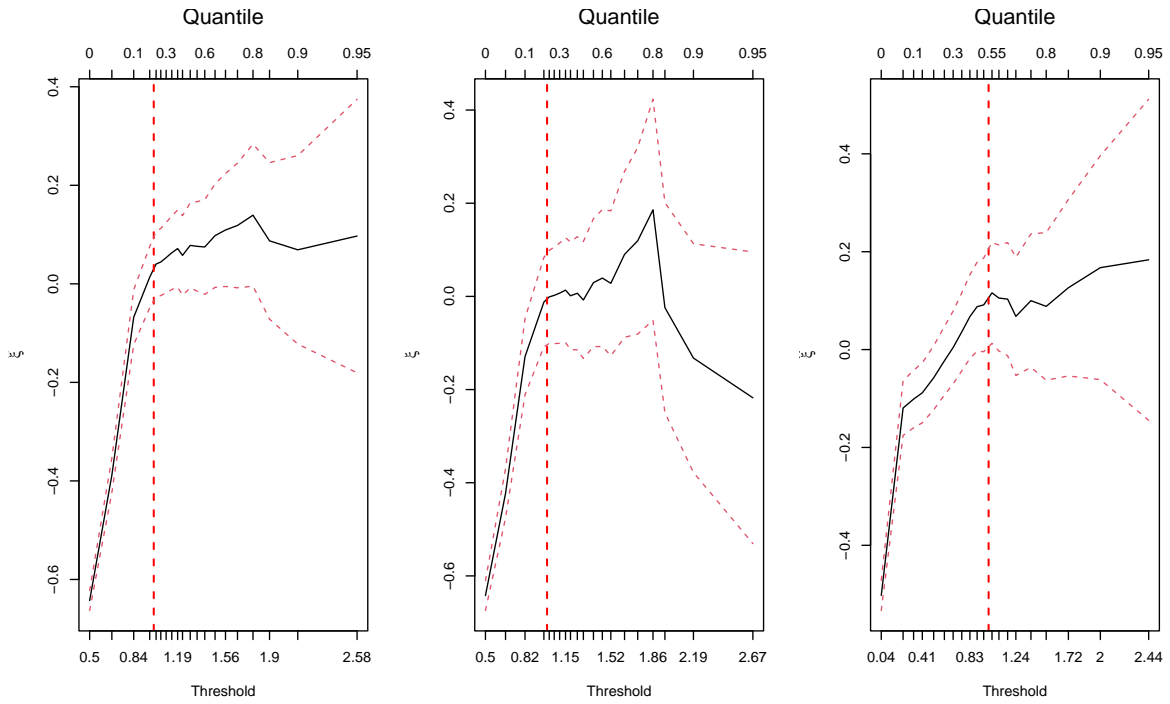


Figure S.1: Examples of parameter stability plots on three simulated datasets used in simulation study in Section 6 of the main text. Solid lines are point estimates (interpolated), dotted lines are pointwise confidence intervals (interpolated), vertical dashed line is the true threshold.

### S:2.3 Northrop and Coleman (2014)

As mentioned in Section 2 of the main text, an example of the plot of  $p$ -values derived from the Northrop and Coleman (2014) method is given in Figure S.2 below. Here, we provide further description of that method and describe some of the inadequacies that limit the applicability of the method and complicate the interpretation of such a plot for threshold selection.

Northrop and Coleman (2014) start by testing the hypothesis that the underlying shape parameter is constant for any threshold above a selected candidate threshold. They extend the piecewise-constant model for the shape parameter, set up in Wadsworth and Tawn (2012), to allow for an arbitrary number of thresholds and avoid the multiple-testing issue.

They derive likelihood ratio and score tests associated with this model to test for equality of the shape parameter estimates above a candidate threshold. The method results in a plot of  $p$ -values against threshold. Each  $p$ -value corresponds to a candidate threshold  $u$  and is the result of a hypothesis test which assesses the invariance of the shape parameter for all thresholds above  $u$ .

Figure S.2 shows a plot of  $p$ -values derived from a sample of 200 random variates generated as in Case 4, described in Section S:4.2, with the true threshold of  $u = 1.0$  (16.67% quantile), plotted as a red dashed line. While the Northrop and Coleman (2014) method was aimed to improve upon the parameter stability plot in terms of interpretability, it still suffers from problems with subjectivity. For example, whether to select the threshold as the smallest candidate threshold for which the  $p$ -value rises above the significance level of, say 0.05, or as the candidate threshold which causes the largest increase in the  $p$ -value. In Figure S.2, using the latter approach would result in a threshold chosen as high as the 85%-quantile, far from the true threshold and leaving only 72 exceedances for the extreme value analysis. In contrast, the former approach results in the chosen threshold being the 15%-quantile which lies near the true value, although the variability of the  $p$ -values above casts doubt on this choice. We want to select a threshold where the  $p$ -values indicate strong evidence for parameter stability for all higher thresholds, excluding very high quantiles where uncertainty may become too large. In Figure S.2, beyond the true threshold, the  $p$ -values decrease and remain at relatively low levels until a spike at the 80%-quantile level. Hence, a user of the Northrop and Coleman (2014) method may choose a higher threshold than the 80%-quantile for this dataset, leaving very few exceedances. The variability in this plot may be due to

the small sample size of the simulated dataset. Whatever the reason, while the Northrop and Coleman (2014) method tackles some of the inadequacies of parameter stability plots, it suffers from similar shortcomings due to the difficulty of interpretation of the resulting plot of  $p$ -values.

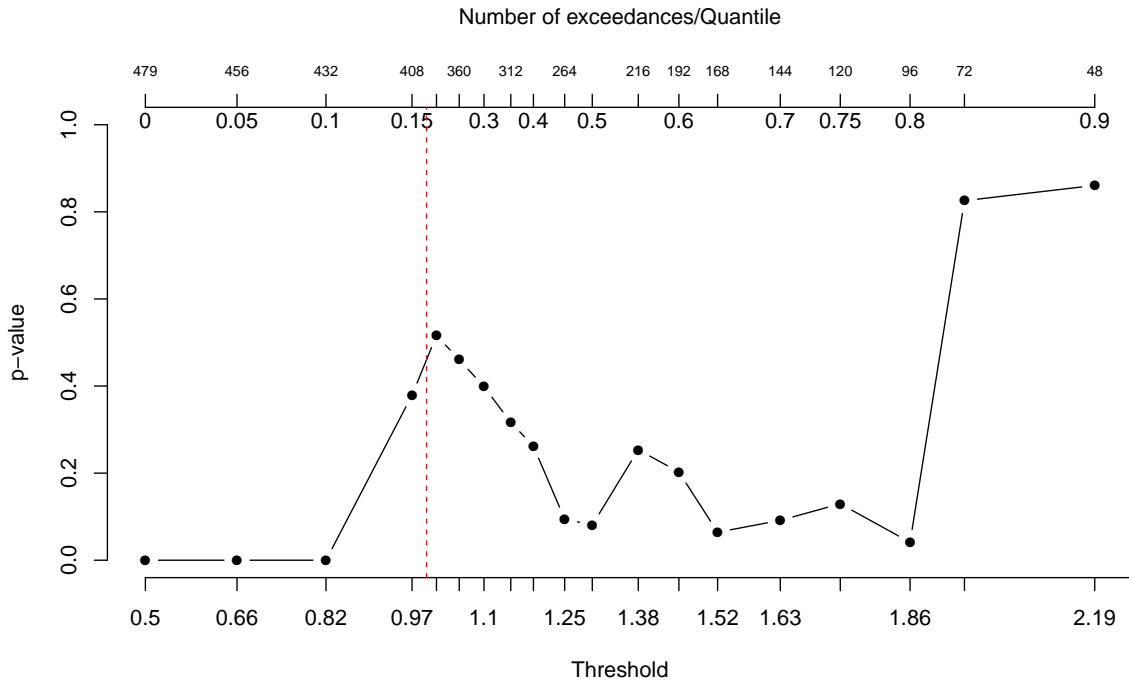


Figure S.2:  $p$ -values derived from Northrop and Coleman (2014) method for threshold selection applied to the second simulated dataset from Figure S.1. Vertical dashed line is the true threshold.

### S:3 Details of current automated methods

We provide a more complete description of the automated threshold selection methods which were outlined in Section 3 of the main paper.

### S:3.1 Wadsworth (2016)

Wadsworth (2016) aims to address the subjective nature of the standard parameter stability plots by utilising the asymptotic distributional theory of the joint distribution of maximum likelihood estimators (MLEs) from samples of exceedances over a range of thresholds. By construction, the exceedances of threshold  $v$  are a subset of that of threshold  $u$  whenever  $v > u$ . Thus, due to this data-overlap, non-standard statistical tests are required. The method aims to output more interpretable diagnostic plots to improve on the difficulties that come with standard parameter stability plots, primarily by removing dependence between estimates at different candidate thresholds. A simple likelihood-based testing procedure is suggested to allow automated selection of the threshold.

Wadsworth (2016) used the point process representation of extremes, derived in Pickands (1971), which considers exceedances of a high threshold  $u$  as a realisation from a non-homeogeneous Poisson process (NHPP). The representation is outlined as follows. Let  $\mathbf{X} = (X_1, \dots, X_n)$  be a sequence of independent random variables with common distribution function  $F$ . Suppose there exists normalising sequences  $\{a_n > 0\}$  and  $\{b_n \in \mathbb{R}\}$  such that the sequence of point processes

$$P_n = \left\{ \left( \frac{i}{n+1}, \frac{X_i - b_n}{a_n} \right) : i = 1, \dots, n \right\} \xrightarrow{d} \mathcal{P} \quad (\text{S.1})$$

as  $n \rightarrow \infty$  with  $\mathcal{P}$  on  $(0, 1) \times (b_l = \lim_{n \rightarrow \infty} (x_F - b_n)/a_n, \infty)$  where  $x_F := \inf\{x : F(x) > 0\}$

is the lower end-point of the support. Then,  $\mathcal{P}$  is a NHPP with intensity:

$$\lambda(t, x) = \frac{1}{\sigma} \left[ 1 + \xi \left( \frac{x - \mu}{\sigma} \right) \right]_+^{-1/\xi}$$

on  $(t, x) \in [0, 1] \times (b_l, \infty)$ .

Now, due to the homogeneity of the process in time, considering regions of the form  $A = (t_1, t_2) \times [u, \infty)$  for  $0 < t_1 < t_2 < 1$  and some threshold  $u > b_l$ , the integrated intensity function on such a region is given by:

$$\Lambda(A) = \int_u^\infty \int_{t_1}^{t_2} \lambda(t, x) \, dt \, dx = (t_2 - t_1) \left[ 1 + \xi \left( \frac{u - \mu}{\sigma} \right) \right]_+^{-1/\xi}$$

with  $\mu \in \mathbb{R}, \sigma > 0, \xi \in \mathbb{R}$  corresponding to the location, scale and shape parameter respectively, with  $\xi$  as in the GPD detailed in Section 1 of the main paper. The parameters of the model are denoted  $\boldsymbol{\theta} \subseteq \mathbb{R}^3$  hereafter, with  $\boldsymbol{\theta}_0$  denoting the true value.

Wadsworth (2016) considers  $\mathbf{X} = (x_1, \dots, x_N)$  as realisations from a NHPP with a random count  $N$  on some region  $R$ , intensity  $\lambda_{\boldsymbol{\theta}}(x)$  and integrated intensity given by  $\Lambda_{\boldsymbol{\theta}}(R) = \int_R \lambda_{\boldsymbol{\theta}}(x) \, dx$ . A set of candidate threshold choices  $(u_1, \dots, u_k)$  with  $u_1 < u_2 \dots < u_k$  are considered with  $R$  taken as the region  $(u_1, \infty)$  and nested regions  $R_1, R_2, \dots, R_k$  in  $R$  such that  $R_j = (u_j, \infty)$  for  $j = 1, \dots, k$ . Thus,  $R_k \subset R_{k-1} \subset \dots \subset R_1 = R$ . Suppose that  $\mathbf{X}$  is sorted such that  $x_i$  is the  $i^{\text{th}}$  largest value, i.e.,  $x_N < \dots < x_j < \dots < x_1$ . Thus, if  $x_1, \dots, x_{N_j}$  are all the observations which lie in the region  $R_j$ , then, there are  $N_j$  observations in the

region  $R_j$ . The likelihood of the process over the region  $R_j$  is then given by:

$$L_{R_j}(\boldsymbol{\theta}) := \left( \prod_{i=1}^{N_j} \lambda_{\boldsymbol{\theta}}(x_i) \right) \exp[-\Lambda_{\boldsymbol{\theta}}(R_j)].$$

Now, we denote the MLE of  $\boldsymbol{\theta}$  based only on the data in region  $R_j$  by  $\hat{\boldsymbol{\theta}}_j$  and the  $3 \times 3$  Fisher information matrix for this likelihood as  $I_j$  with  $I_j^{-1}$  its inverse. Based on asymptotic theory, Wadsworth (2016) considers a superposition of  $m$  Poisson processes as  $m \rightarrow \infty$  giving the following result:

$$m^{1/2} \left( \hat{\boldsymbol{\theta}}_1 - \boldsymbol{\theta}_0, \hat{\boldsymbol{\theta}}_2 - \boldsymbol{\theta}_0, \dots, \hat{\boldsymbol{\theta}}_k - \boldsymbol{\theta}_0 \right)^T \xrightarrow{d} N_{3k}(\mathbf{0}, \Sigma),$$

with  $\Sigma$  the  $3k \times 3k$  covariance matrix given by  $\Sigma = (I_{\min(i,j)}^{-1})_{1 \leq i \leq k, 1 \leq j \leq k}$ .

Wadsworth (2016) uses the above result to construct a threshold selection procedure. Isolating the shape parameter  $\xi$  in the inference, then  $m^{-1}\{(I_{j+1}^{-1} - I_j^{-1})_{\xi, \xi}\}$  is the asymptotic variance of the estimated increment  $\hat{\xi}_j - \hat{\xi}_{j+1}$  where  $\hat{\xi}_j$  is the MLE of the shape parameter on the region  $R_j$ . As these increments have changing variance with  $j$ , consider the standardised increments  $\hat{\boldsymbol{\xi}}^* = (\hat{\xi}_1^*, \dots, \hat{\xi}_{k-1}^*)^T$  given by:

$$\left( \hat{\xi}_1^*, \hat{\xi}_2^*, \dots, \hat{\xi}_{k-1}^* \right)^T := m^{1/2} \left( \frac{\hat{\xi}_1 - \hat{\xi}_2}{((I_2^{-1} - I_1^{-1})_{\xi, \xi})^{1/2}}, \frac{\hat{\xi}_2 - \hat{\xi}_3}{((I_3^{-1} - I_2^{-1})_{\xi, \xi})^{1/2}}, \dots, \frac{\hat{\xi}_{k-1} - \hat{\xi}_k}{((I_k^{-1} - I_{k-1}^{-1})_{\xi, \xi})^{1/2}} \right)^T, \quad (\text{S.2})$$

as these have common unit variances over all components. It follows that if the excesses of  $u_1$  follow a GPD then, as  $m \rightarrow \infty$ ,  $\hat{\boldsymbol{\xi}}^* \rightarrow \mathbf{Z}$  where  $\mathbf{Z} \sim N_{k-1}(\mathbf{0}, \mathbf{1}_{k-1})$  with  $\mathbf{1}_n$  denoting the  $n \times n$ -dimensional identity matrix. Given these properties, Wadsworth (2016) term  $\hat{\boldsymbol{\xi}}^*$  as a

white-noise process.

As a result of the penultimate theory of extremes, described by Smith (1987) and Gomes (1994), Wadsworth (2016) explains that departures from the null assumption of the white-noise process described in (S.2) are a direct consequence of too many values from the body of the data (where the GPD is not appropriate) being included in the estimation. This logic suggests that below the appropriate threshold, say  $u_j$ , the variables  $\xi_i^*$ ,  $i = 1, \dots, j-1$  might be better approximated by a  $N(\beta, \gamma^2)$  than by a standard normal distribution which is the limit distribution if the threshold  $u_j$  was correct. Formally, this gives a changepoint model as:

$$\xi_i^* \sim N(\beta, \gamma^2) \quad iid, \quad i = 1, \dots, j-1, \quad \xi_i^* \sim N(0, 1) \quad iid, \quad i = j, \dots, k-1,$$

where  $j, \beta, \gamma$  are unknown.

Wadsworth (2016) maximise the profile likelihood for  $\beta$  and  $\gamma$  across  $j$  and use a likelihood ratio test to assess if this gives a significantly better fit to  $\hat{\xi}^*$  than the standard normal distribution. A threshold is automatically selected as the candidate threshold  $u_j$  which provides the best fit. If there is no evidence of  $\hat{\xi}^*$  deviating from white-noise, then the lowest candidate threshold is selected, i.e.,  $u_1$  in this case.

### S:3.2 Northrop et al. (2017)

Consider  $\mathbf{X} = (X_1, \dots, X_n)$  where  $X_i$  are iid and have associated realisations  $\mathbf{x} = (x_1, \dots, x_n)$ . Northrop et al. (2017) assume, without loss of generality, that the realisations have the prop-

erty  $x_1 < \dots < x_n$ . This contrasts with the setup for the Wadsworth (2016) method, however, we keep this to stay aligned with Northrop et al. (2017) in our explanation. Northrop et al. (2017) consider  $u$  as a training threshold and allow for the threshold exceedance rate, denoted  $\lambda_u = \mathbb{P}(X > u)$ , to be incorporated with the GPD parameters  $(\sigma_u, \xi)$  into the fit. Thus,  $\boldsymbol{\theta} = (\lambda_u, \sigma_u, \xi)$  and subsequently, in this section, we refer to the tail model as the  $\text{GPD}(\lambda_u, \sigma_u, \xi)$ . Let  $\pi_u(\boldsymbol{\theta})$  be a prior density for  $\boldsymbol{\theta}$ . Let  $\mathbf{x}_{(-r)} = \{x_i, i \neq r\}$ . The posterior density for  $\boldsymbol{\theta}$  given data  $\mathbf{x}_{(-r)}$  is denoted  $\pi_u(\boldsymbol{\theta}|\mathbf{x}_{(-r)})$  with  $\pi_u(\boldsymbol{\theta}|\mathbf{x}_{(-r)}) \propto L(\boldsymbol{\theta}; \mathbf{x}_{(-r)}, u) \pi_u(\boldsymbol{\theta})$  and the likelihood is assumed to take the form:

$$L(\boldsymbol{\theta}; \mathbf{x}_{(-r)}, u) = \prod_{i: x_i \in \mathbf{x}_{(-r)}} f_u(x_i | \boldsymbol{\theta}), \quad (\text{S.3})$$

$$f_u(x | \boldsymbol{\theta}) = (1 - \lambda_u)^{I(x \leq u)} [\lambda_u h(x - u; \sigma_u, \xi)]^{I(x > u)},$$

where  $I(w)$  is an indicator function giving 1 if  $w$  is true and 0 otherwise, and  $h(x; \sigma_u, \xi) = \sigma_u^{-1} [1 + \xi x / \sigma_u]_+^{-(1+1/\xi)}$  is the density of a GPD as in Section 1 of the main text. In the case of  $\lambda_u = 0$ ,  $f_u(x_r | \boldsymbol{\theta}) = I(x_r \leq u)$ . Note that, as defined,  $f_u(x | \boldsymbol{\theta})$  is not a valid density function as it integrates to  $\infty$  and it is discontinuous at  $x = u$ . The use of the term “density” is identified in Northrop et al. (2017) as an abuse of terminology.

Northrop et al. (2017) aim to compare a set of candidate values for  $u$ , denoted  $(u_1, \dots, u_k)$  with  $u_1 < \dots < u_k$ , by introducing a fixed validation threshold  $v \geq u$  and quantifying the predictive ability of the implied  $\text{GPD}(\lambda_v, \sigma_v, \xi)$  using each candidate threshold  $u_i, i = 1, \dots, k$ . Since  $v$  is fixed, the performance of each of the candidate thresholds is compared based on the same validation data. To undertake such comparisons over thresholds, a slight extension of the threshold stability property, stated in Section 2 of the main paper, is required, i.e.,

if a  $\text{GPD}(\lambda_u, \sigma_u, \xi)$  tail model applies at  $u$ , this implies a  $\text{GPD}(\lambda_v, \sigma_v, \xi)$  tail model above  $v$  where  $\sigma_v = \sigma_u + \xi(v - u)$  and  $\lambda_v = \lambda_u[1 + \xi(v - u)/\sigma_u]^{-1/\xi}$  assuming that  $v$  is such that  $1 + \xi(v - u)/\sigma_u > 0$ .

For the cross-validation scheme,  $\mathbf{x}_{(-r)}$  is the training data with  $x_r$  the validation data for each  $r = 1, \dots, n$ . To assess the threshold choice performance above  $v$ , they use leave-one-out cross-validation. The cross-validation predictive density for level  $v$  under model (S.3), using training threshold  $u_j$ ,  $j = 1, \dots, k - 1$ , is then given by:

$$f_v(x_r | \mathbf{x}_{(-r)}, u_j) = \int f_v(x_r | \boldsymbol{\theta}) \pi_{u_j}(\boldsymbol{\theta} | \mathbf{x}_{(-r)}) d\boldsymbol{\theta}, \quad r = 1, \dots, n.$$

Northrop et al. (2017) discuss the additional choice of  $v$  required by the method, with  $v \geq u_k$  being necessary. The higher that  $v$  is chosen, the fewer excesses of  $v$ , resulting in less information gained to distinguish between the lower threshold choices, so they decide to use  $v = u_k$ .

A Monte Carlo estimator for approximating  $f_v(x_r | \mathbf{x}_{(-r)}, u)$  uses the MCMC sampling realisations  $\boldsymbol{\theta}_j^{(-r)}, j = 1, \dots, m$  from the posterior distribution  $\pi_u(\boldsymbol{\theta} | \mathbf{x}_{(-r)})$  through:

$$\hat{f}_v(x_r | \mathbf{x}_{(-r)}, u) = \frac{1}{m} \sum_{j=1}^m f_v(x_r | \boldsymbol{\theta}_j^{(-r)}), \quad r = 1, \dots, n.$$

This leads to a measure of predictive ability at  $v$  given by:

$$\hat{T}_v(u) = \sum_{r=1}^n \log\{\hat{f}_v(x_r | \mathbf{x}_{(-r)}, u)\}$$

which is evaluated over all choices of  $u_1, \dots, u_k$  for  $u$ . Out of these candidate thresholds,

Northrop et al. (2017) select the one which maximises the measure,  $\hat{T}_v$ .

To improve the computational efficiency of the estimator  $\hat{f}_v(x_r | \mathbf{x}_{(-r)}, u)$  for  $r = 1, \dots, n$ ,

Northrop et al. (2017) use an importance sampling ratio estimator of Gelfand (1996). This

allows for estimation over  $r$  using a single sample from the posterior distribution  $\pi_u(\boldsymbol{\theta} | \mathbf{x})$ .

Specifically, for a single sample  $\{\boldsymbol{\theta}_j, j = 1, \dots, m\}$  from the posterior  $\pi_u(\boldsymbol{\theta} | \mathbf{x})$ ,

$$\hat{f}_v(x_r | \mathbf{x}_{(-r)}, u) = \frac{\sum_{j=1}^m f_v(x_r | \boldsymbol{\theta}_j) q_r(\boldsymbol{\theta}_j)}{\sum_{j=1}^m q_r(\boldsymbol{\theta}_j)} = \frac{\sum_{j=1}^m f_v(x_r | \boldsymbol{\theta}_j) / f_u(x_r | \boldsymbol{\theta}_j)}{\sum_{j=1}^m 1 / f_u(x_r | \boldsymbol{\theta}_j)}$$

by taking  $q_r(\boldsymbol{\theta}) = \pi_u(\boldsymbol{\theta} | \mathbf{x}_{(-r)}) / \pi_u(\boldsymbol{\theta} | \mathbf{x}) \propto 1 / f_u(x_r | \boldsymbol{\theta})$ .

## S:4 Extra simulation study results for Section 6

For Cases 1-4 studied in Section 6 of the main paper, we present further simulation experiments to assess the performance of the EQD against existing methods as well as an additional breakdown of some of the results discussed in Section 6 of the main text. We also outline a study that was conducted to compare EQD against the Varty et al. (2021) method.

### S:4.1 Comparison with Varty et al. (2021)

Figure S.3 shows the results from an experiment comparing the EQD against the Varty et al. (2021) method in terms of threshold selection in the case of iid simulated GPD data in excess of a threshold of  $u = 1.0$  and in terms of the accuracy of quantile estimation for simulated

Gaussian data, where there is no true threshold above which a GPD is an exact description of the distribution. Thus, the first case is the idealistic case of GPD samples above a known threshold with no values lying below  $u$  whereas the second case corresponds to a distribution with well known slow convergence to extreme value limits.

We simulated 30 repeated GPD samples of size  $n$  with  $n = 1000 - 50000$ . The data are generated from a GPD above  $u$  with no data values lying below  $u$ , although candidate thresholds below  $u$  are considered. We compared the difference in the absolute error from the true threshold of  $u = 1.0$  for each method. The results are shown in Figure S.3 (left) where points below (above) 0 represent cases where the EQD performed better (worse) than the Varty et al. (2021) method, points at the line 0 represented by large, open points correspond to cases where there was no difference. The size of the points in this plot corresponds to the number of times an absolute error of that value was obtained. The plot shows that, for the GPD samples, the EQD tends to have a smaller absolute error outperforming (underperforming) the Varty et al. (2021) method on 8.7% (0.7%) of samples, while equal in error for 90.5% of the samples. In general, the additional error in the Varty et al. (2021) method comes from underestimation of the thresholds.

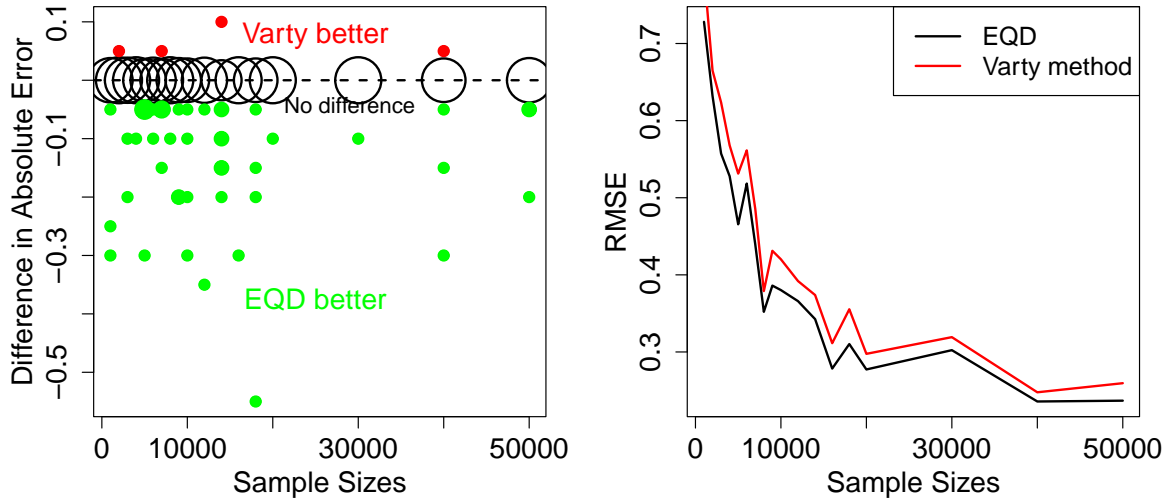


Figure S.3: IID Case Study: [Left] Difference in absolute error from true threshold  $u = 1.0$  for EQD and Varty et al. (2021) methods applied to 30 simulated GPD samples of sample size ranging from  $n = 1000$  to  $n = 50000$ . The size of the points represents the number of times an absolute error of that value was seen for a certain sample size. [Right] RMSE of estimates of  $(1-10^{-5})$ -quantile based on GPD fit to Gaussian data using threshold choice from EQD and Varty et al. (2021) methods for 30 samples of Gaussian data of sample size ranging from  $n = 1000$  to  $n = 50000$ .

Figure S.3 (right) also shows the RMSE of a quantile estimate from a simulation of 30 repeated samples of Gaussian data for sample sizes  $n = 1000 - 50000$ . Here, there is no true threshold and so, comparison is made based on quantile estimation using the fitted GPD above the chosen threshold in each case. We compare the resulting quantile estimates for an exceedance probability of  $p = 10^{-5}$  to the true quantile of a standard normal distribution and obtain RMSEs of quantile estimates across the 30 samples for each sample size. While the estimated RMSE generally decreases as  $n$  increases, our method tends to have a smaller RMSE than the Varty et al. (2021) method across all sample sizes. We obtained results across a range of exceedance probabilities and found similar conclusions.

Tables S.1 and S.2 break down the RMSE into the bias and variance components for three of the sample sizes illustrated in Figure S.3. The smallest RMSE in each case is highlighted in bold. The variance component is very similar across both methods so the ordering of RMSE values is due to the larger bias in the Varty et al. (2021) method; a result of the method's tendency to select lower thresholds than the EQD. This is reiterated in Table S.2 where the added bias from the Exponential(1) transformation causes larger RMSE values of the estimated quantile at the exceedance probability of  $10^{-5}$  across the three sample sizes.

<i>n</i>	EQD			Varty method		
	RMSE	Bias	Variance	RMSE	Bias	Variance
1000	<b>0.094</b>	0.047	0.007	0.107	0.050	0.009
10000	<b>0.132</b>	0.035	0.016	0.133	0.038	0.016
40000	<b>0.058</b>	0.027	0.002	0.081	0.033	0.005

Table S.1: Bias and variance decomposition of RMSE in estimated threshold of EQD and Varty et al. (2021) methods for simulated GPD data.

<i>n</i>	EQD			Varty method		
	RMSE	Bias	Variance	RMSE	Bias	Variance
1000	<b>0.728</b>	0.626	0.139	0.793	0.703	0.135
10000	<b>0.380</b>	0.252	0.081	0.420	0.305	0.083
40000	<b>0.236</b>	0.166	0.028	0.248	0.181	0.029

Table S.2: Bias and variance decomposition of RMSE for estimated  $(1 - p)$ -quantile for  $p = 10^{-5}$  using fitted GPD above chosen threshold from EQD and Varty et al. (2021) methods for simulated Gaussian data.

Based on this small case study, we conclude that there is no merit in including the Varty et al. (2021) method when the data are iid, so we omit this approach from the simulation study discussed in Section 6 of the main text.

## S:4.2 Case 1-4 distributions and quantile calculations

This section provides the distribution functions and true quantile calculations used for the simulated samples in Cases 1-4 in Section 6 of the main paper.

*Case 1-3:* We simulate from a mixture of a Uniform(0.5, 1.0) distribution and a GPD( $\sigma_u, \xi$ ) distribution above the threshold  $u = 1.0$ . Model parameters and sample sizes are given in Table 1 of Section 6 in the main paper. The simulated samples come from a distribution with distribution function:

$$F_X(x) = \begin{cases} \frac{x-0.5}{3}, & 0.5 \leq x \leq 1 \\ \frac{1}{6} + \frac{5}{6} [H(x-1; \sigma_u, \xi)], & x > 1. \end{cases} \quad (\text{S.4})$$

where  $H(x-1; \sigma_u, \xi)$  is the distribution function of a GPD with parameters  $(\sigma_u, \xi)$ .

For a distribution given by expression (S.4), the true quantile  $x_p$  at exceedance probability  $p$  (for  $p < 5/6$ ) is given by:

$$x_p = 1 + \frac{\sigma_u}{\xi} \left[ \left( \frac{6p}{5} \right)^{-\xi} - 1 \right]$$

where  $(\sigma_u, \xi)$  are the selected GPD scale and shape parameters.

*Case 4:* We simulate a proposal variable  $Y \sim \text{GPD}(0.5, 0.1)$  above the threshold  $u = 0$ , but below  $u = 1.0$ , we reject values of  $Y$  if they lie below random variates generated from variable  $B \sim \text{Beta}(1, 0.5)$ , i.e., if  $Y < B$ . We repeat this procedure until we have a sample

of size 1000. The simulated samples come from a distribution with distribution function:

$$F_X(x) = \begin{cases} \int_0^x h(x; 0.5, 0.1) \mathbb{P}(B < x) dx, & 0 \leq x \leq 1 \\ q + (1 - q) [H(x - 1; 0.5, 0.1)], & x > 1, \end{cases} \quad (\text{S.5})$$

where  $H(x - 1; 0.5, 0.1)$  and  $h(x; 0.5, 0.1)$  are the distribution and corresponding density functions of a GPD with parameters  $(0.5, 0.1)$  and  $q = \int_0^1 h(x; 0.5, 0.1) \mathbb{P}(B < x) dx$ . We choose the distribution of  $B$  so that the resulting sample has a mode below 1.0 but a GPD tail above 1.0. Only  $q$  is relevant for evaluating quantiles above 1.0, with  $q$  estimated to a high degree of accuracy using Monte Carlo methods.

For the distribution given in expression (S.5), the true quantile  $x_p$  at exceedance probability  $p$  is:

$$x_p = 1 + \frac{\sigma_1}{\xi} \left[ \left( \frac{p}{1 - q} \right)^{-\xi} - 1 \right]$$

where  $\sigma_1 = \sigma + \xi$  with  $\sigma = 0.5$  and  $\xi = 0.1$  the underlying scale and shape parameter and  $q \approx 0.5290265$ .

Examples of one of the simulated datasets from each of Cases 1-4 are given in Figure S.4. The histograms show that the GPD tails (i.e., above 1.0) are a large proportion of each sample. This is unusual in practice and so threshold selection should be easier in these examples than typically. This is especially true for Cases 1-3 with the density having a step change at the threshold. The idea behind our choice of distributions is that if methods struggle in cases where we have a clear true threshold then there will be significant problems when it comes to real datasets.

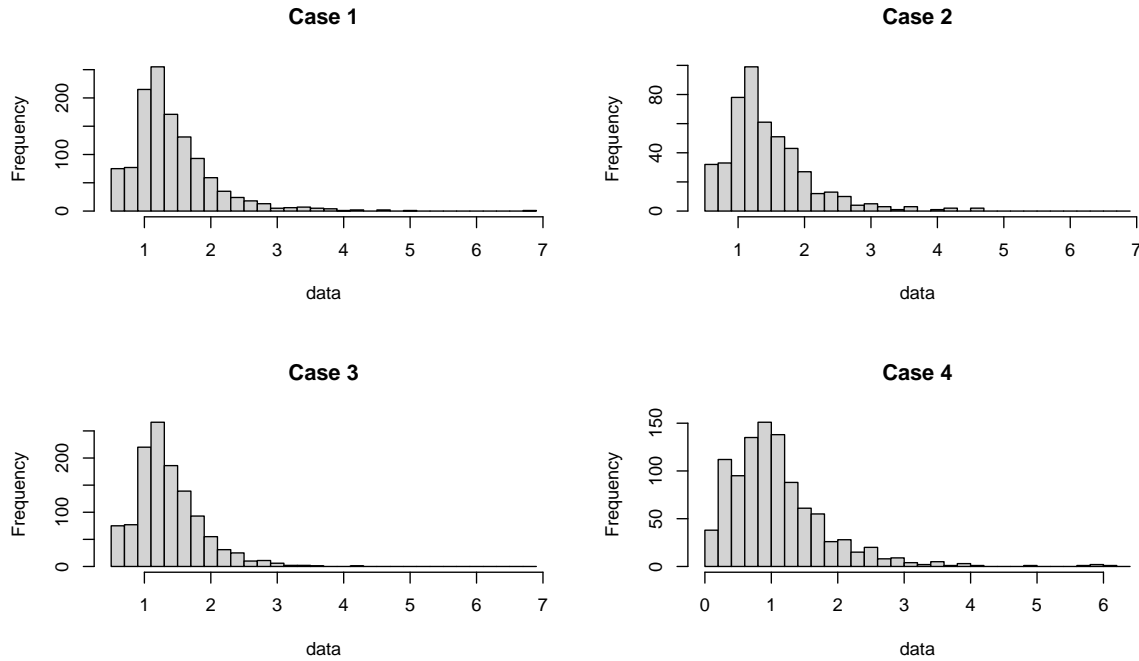


Figure S.4: Histograms of simulated dataset examples from Cases 1-4.

### S:4.3 Further case studies

This section provides a description and the results of case studies further to Case 1-4 which were omitted from Section 6 in the main paper. In the following cases, the Wadsworth (2016) failed to estimate a threshold for a large portion of the simulated samples. This high failure rate occurs for two reasons; dependence between parameter estimates when using candidate thresholds which lie in close proximity for small sample sizes or in the cases where  $\xi < -0.05$ , where an error results from a divergent integral in the calculation of the inverse Fisher information matrix. Thus, we omitted these cases from the main paper and only show comparisons of our method against the Northrop et al. (2017) method here.

*Case 2A:* We simulate samples from the distribution (S.4) but with a reduced sample size of 120.

*Case 3A & 3B:* We simulate samples from the distribution (S.4) but with shape parameters  $\xi < -0.05$ ,  $\xi = -0.2$  for Case 3A and  $\xi = -0.3$  for Case 3B.

Table S.3 shows the RMSEs of the EQD and the Northrop et al. (2017) method for estimating the threshold in Case 2A, 3A and 3B. The smallest RMSE in each case is given in bold. Outside of uncertainty due to the small sample size in Case 2A, our method performs well and achieves a high degree of accuracy. This is important as having a small number of exceedances is most common when modelling the tail of a distribution. In contrast, Northrop et al. (2017) gives highly variable results. Overall, our method achieves a smaller (equal) absolute error in threshold in 74.0% (12.8%) of samples. In Case 3A and 3B, our method obtains adequate results with a significantly lower RMSE than the Northrop method. The EQD obtains a smaller (equal) absolute error in 51.5% (22.6%) of samples in Case 3A and 50.4% (19.6%) in Case 3B.

	Case 2A	Case 3A	Case 3B
<i>EQD</i>	<b>0.162</b>	<b>0.117</b>	<b>0.210</b>
<i>Northrop</i>	0.655	0.342	0.360

Table S.3: RMSEs of the threshold choices of the EQD and Northrop methods in Cases 2A, 3A and 3B.

#### S:4.4 Detailed results from simulation study

This section provides the RMSE results with corresponding bias and variance components for all methods described in Section 3 of the main text.

#### S:4.4.1 Scenario 1: True GPD tail

Table S.4 shows the RMSEs of the estimated thresholds as well as bias and variance decomposition for Cases 1-4. To reiterate Section 6 of the main paper, in Cases 1-4, the EQD achieves the smallest RMSEs, the least variable results and the least biased threshold estimates. In Table S.5, the results for the Danielsson et al. (2001) and Danielsson et al. (2019) methods are shown. Both approaches achieve considerably larger RMSEs than all other methods. In Case 3, the Danielsson et al. (2001) method exhibits lower variability in the estimated thresholds than other cases but incurs very large bias due to over-estimation, with a RMSE 42.13 times larger than that of the EQD. Using this method results in large variability and significant bias in all cases, leading to the largest RMSEs of all the analysed methods. In all cases, the Danielsson et al. (2019) method shows low variability in the threshold estimates but incurs a large amount of bias, leading to very large RMSE values.

Case	EQD			Wadsworth <sup>5</sup>			Northrop		
	RMSE	Bias	Variance	RMSE	Bias	Variance	RMSE	Bias	Variance
Case 1	<b>0.048</b>	<b>0.034</b>	<b>0.001</b>	0.349	0.111	0.109	0.536	0.276	0.211
Case 2	<b>0.060</b>	<b>0.031</b>	<b>0.003</b>	0.461	0.204	0.171	0.507	0.238	0.201
Case 3	<b>0.060</b>	<b>0.042</b>	<b>0.002</b>	0.221	0.060	0.045	0.463	0.256	0.149
Case 4	<b>0.101</b>	<b>-0.071</b>	<b>0.005</b>	0.411	0.090	0.161	0.497	0.150	0.225

Table S.4: RMSE, bias and variance of the threshold choices for each of the methods used in Cases 1-4.

Tables S.6 & S.7 present the bias and variance of the estimation of  $(1 - p_j)$ -quantiles where  $p_j = 1/(10^j n)$  for  $j = 0, 1, 2$  with  $n$  denoting the length of the simulated dataset for the EQD, Wadsworth (2016) and Northrop et al. (2017) methods applied in Cases 1-4. As mentioned in Section 6 of the main paper, we use exceedance probabilities of this form as we have

<sup>5</sup>Results for Wadsworth are calculated only on the samples where a threshold was estimated. It failed estimate a threshold for 2.4%, 26.4%, 0%, 4.6% of the simulated samples in Cases 1-4, respectively.

	<i>Danielsson et al. (2001)</i>			<i>Danielsson et al. (2019)</i>		
Case	RMSE	Bias	Variance	RMSE	Bias	Variance
Case 1	2.767	2.416	1.822	1.635	1.633	0.007
Case 2	2.212	1.850	1.471	1.639	1.634	0.017
Case 3	2.528	2.441	0.434	1.314	1.314	0.001
Case 4	2.989	2.628	2.028	1.532	1.528	0.012

Table S.5: RMSE, bias and variance of the threshold choices for each of the Danielsson et al. (2001) and Danielsson et al. (2019) methods used in Cases 1-4.

simulated samples of different sizes and want to make extrapolation equally difficult in each case. While the smallest values in Table S.6 vary between each of the methods, the EQD incurs the least bias in the majority of cases and quantiles. In particular, the EQD achieves the smallest values, for all  $j$ , in Cases 2 and 3. Furthermore, in Table S.7, the EQD shows the least variability in quantile estimates for all  $j$  in all cases, with differences made more evident with higher  $j$ .

	<i>EQD</i>	<i>Wadsworth<sup>5</sup></i>	<i>Northrop</i>	<i>EQD</i>	<i>Wadsworth<sup>5</sup></i>	<i>Northrop</i>
$j$	<b>Case 1</b>			<b>Case 2</b>		
0	<b>-0.021</b>	-0.079	-0.075	<b>-0.049</b>	-0.118	-0.071
1	-0.015	-0.192	<b>-0.001</b>	<b>-0.046</b>	-0.316	0.245
2	<b>0.044</b>	-0.319	0.554	<b>0.069</b>	-0.532	2.568
	<b>Case 3</b>			<b>Case 4</b>		
0	<b>-0.008</b>	-0.026	-0.041	-0.092	-0.049	<b>-0.081</b>
1	<b>-0.007</b>	-0.047	-0.065	-0.231	-0.137	<b>-0.022</b>
2	<b>-0.002</b>	-0.066	-0.074	-0.389	<b>-0.144</b>	0.645

Table S.6: Bias of the estimated quantiles in Cases 1-4 based on fitted GPD above chosen threshold. The smallest absolute bias for each quantile are highlighted in bold.

Table S.8 presents the RMSEs for  $(1-p_j)$ -quantiles where  $p_j = 1/(10^j n)$  for  $j = 0, 1, 2$  with  $n$  denoting the length of the simulated dataset for the Danielsson et al. (2001) and Danielsson et al. (2019) methods applied in Cases 1-4. For  $j = 0$ , the threshold choice should not be too important as we are not extrapolating but even in this case, Table S.8 shows that both

	<i>EQD</i>	<i>Wadsworth</i> <sup>5</sup>	<i>Northrop</i>	<i>EQD</i>	<i>Wadsworth</i> <sup>5</sup>	<i>Northrop</i>
<i>j</i>	Case 1			Case 2		
0	<b>0.316</b>	0.347	0.564	<b>0.357</b>	0.385	0.537
1	<b>1.582</b>	1.899	5.646	<b>2.211</b>	2.604	12.280
2	<b>5.988</b>	7.282	50.055	<b>9.723</b>	11.853	518.530
	Case 3			Case 4		
0	<b>0.036</b>	0.037	0.051	<b>0.462</b>	0.601	0.731
1	<b>0.105</b>	0.116	0.198	<b>2.666</b>	3.965	7.616
2	<b>0.233</b>	0.262	0.548	<b>11.207</b>	17.756	76.789

Table S.7: Variance of the estimated quantiles in Cases 1-4 based on fitted GPD above chosen threshold. The smallest variance for each quantile are highlighted in bold.

the Danielsson et al. (2001) and Danielsson et al. (2019) approaches obtain larger RMSE values than the other methods analysed in Section 6 of the main paper. This difference is only exacerbated as we extrapolate further. For  $j = 1, 2$ , both approaches lead to RMSEs orders of magnitude larger than any of the other methods analysed.

<i>j</i>	<i>Danielsson 2001</i>	<i>Danielsson 2019</i>	<i>Danielsson 2001</i>	<i>Danielsson 2019</i>
	Case 1		Case 2	
0	1.020	0.859	0.962	0.757
1	3.128	3.172	3.806	3.991
2	12.943	10.303	110.347	23.102
	Case 3		Case 4	
0	0.675	0.262	1.050	0.883
1	1.655	0.570	3.203	3.193
2	38.001	1.000	12.914	10.239

Table S.8: RMSEs in the estimated quantiles in Cases 1-4 based on fitted GPD above chosen threshold for the Danielsson et al. (2001) and Danielsson et al. (2019) methods.

#### S:4.4.2 Scenario 2: Gaussian data

Tables S.9 & S.10 present the RMSE, bias and variance, respectively, of the estimation of  $(1 - p_j)$ -quantiles where  $p_j = 1/(10^j n)$ , for  $j = 0, 1, 2$  in the case of simulated Gaussian data with  $n = 2000, 20000$  as detailed in Section 6 of the main paper. The smallest RMSE,

absolute bias, and variance in each table are shown in bold. For  $n = 2000$ , the EQD achieves the smallest RMSEs for all  $j$ . The Northrop method incurs the least bias in quantile estimation due to its slightly higher threshold choices, shown in Table S.11 which gives the median and 95% CI of the chosen thresholds for each method. However, the EQD exhibits the least variance in the estimated quantiles in all cases which contributes to a lower RMSE for all quantile levels. For the larger samples, this reduction in bias from the Northrop method plays a larger role and contributes to the lowest RMSEs in this case, with the EQD still achieving the least variable results.

$j$	EQD			Wadsworth <sup>6</sup>			Northrop		
	RMSE	Bias	Variance	RMSE	Bias	Variance	RMSE	Bias	Variance
0	<b>0.214</b>	-0.086	<b>0.038</b>	0.249	-0.124	0.047	0.225	<b>-0.076</b>	0.045
1	<b>0.430</b>	-0.275	<b>0.109</b>	0.538	-0.372	0.151	0.461	<b>-0.224</b>	0.162
2	<b>0.703</b>	-0.521	<b>0.222</b>	0.896	-0.663	0.364	0.765	<b>-0.414</b>	0.414

Table S.9: RMSE, bias and variance of estimated  $(1 - p_j)$ -quantiles for 500 replicated samples from a Gaussian distribution with sample size of 2000.

$j$	EQD			Wadsworth			Northrop		
	RMSE	Bias	Variance	RMSE	Bias	Variance	RMSE	Bias	Variance
0	0.187	-0.131	<b>0.018</b>	0.214	-0.165	0.019	<b>0.172</b>	<b>-0.104</b>	0.019
1	0.368	-0.307	<b>0.042</b>	0.422	-0.366	0.044	<b>0.331</b>	<b>-0.255</b>	0.045
2	0.594	-0.528	<b>0.074</b>	0.672	-0.611	0.078	<b>0.533</b>	<b>-0.450</b>	0.081

Table S.10: RMSE, bias and variance of estimated  $(1 - p_j)$ -quantiles for 500 replicated samples from a Gaussian distribution with sample size of 20000.

	$n = 2000$			$n = 20000$		
	EQD	Wadsworth <sup>6</sup>	Northrop	EQD	Wadsworth	Northrop
Median $Q$	75	50	80	87.5	84	91.5
95% CI $Q$	55, 90	50, 95	60, 95	77.5, 94	69.5, 95	82.5, 95

Table S.11: Median and 95% CI of quantile level  $Q$  (%) for the threshold choices for each method over 500 replicated samples from a Gaussian distribution for two sample sizes  $n$ .

<sup>6</sup>Results for the Wadsworth method, which failed on 0.4% of the samples here, are calculated only for samples where a threshold estimate was obtained.

Table S.12 shows the results of the quantile estimation using the Danielsson et al. (2001) and Danielsson et al. (2019) methods for the 500 replicated standard Gaussian samples with  $n = 2000$ . For Gaussian data, the Danielsson et al. (2019) method actually incurs the lowest bias of all analysed methods in its estimated quantiles for all  $j$ , most likely due to threshold choices being pushed into the tail. The reason for this is that the method does not take sampling variability into account when selecting a threshold and as a result, the reduction in bias in the GPD fit at higher thresholds drives the choice further into the tail. However, the method shows significant variability in its quantile estimates which leads to higher RMSEs than the EQD and Northrop methods. The Danielsson et al. (2001) method incurs considerable bias with large variance in its quantile estimates, leading to the highest RMSEs of all analysed methods.

$j$	<i>Danielsson et al. (2001)</i>			<i>Danielsson et al. (2019)</i>		
	RMSE	Bias	Variance	RMSE	Bias	Variance
0	0.758	-0.470	0.354	0.232	<b>-0.059</b>	0.050
1	1.550	-0.815	1.739	0.479	<b>-0.173</b>	0.200
2	33.183	-1.380	1099.182	0.790	<b>-0.321</b>	0.522

Table S.12: RMSE, bias and variance of estimated  $(1 - p_j)$ -quantiles for 500 replicated samples from a Gaussian distribution with sample size of 2000 for the Danielsson et al. (2001) and Danielsson et al. (2019) methods.